Meso Stereoisomer as a Probe of Enantioselective Threading Intercalation of Semirigid Ruthenium Complex [μ-(11,11′-bidppz)(phen)$_4$Ru$_2$]$^{4+}$

L. Marcus Wilhelmsson, Elin K. Esbjörner, Fredrik Westerlund, Bengt Nordén, and Per Lincoln*

Physical Chemistry Section at the Department of Chemistry and Bioscience, Chalmers University of Technology, SE−41296 Gothenburg, Sweden

Received: August 5, 2003

Upon interaction with calf thymus DNA the Δ,Δ-enantiomer of the semirigid binuclear ruthenium complex [μ-(11,11′-bidppz)(phen)$_4$Ru$_2$]$^{4+}$ has previously been shown to reorganize from an initial groove bound geometry into an intercalative binding mode, threading one of its bulky Ru(phen)$_2$ moieties through the core of the DNA. We have now found that all three stereoisomers, Δ,Δ; Λ,Λ; and Δ,Λ (meso), are intercalated in their final modes of binding to calf thymus DNA, poly(dA-dT)$_2$, poly(dG-dC)$_2$, as well as poly(dI-dC)$_2$ indicated by linear dichroism, circular dichroism, and luminescence. For all three stereoisomers, studied in detail with poly(dA-dT)$_2$, the bridging bidppz ligand is intercalated in anti conformation, leaving one Ru(phen)$_2$ moiety in each groove. This final binding geometry is characterized by a distinct clockwise roll of the Ru(phen)$_2$ moiety in the minor groove, similar to the roll earlier observed for the dppz ligand in [Ru(phen)$_2$dppz]$^{2+}$. Using the meso stereoisomer as an enantioselective probe, it is shown that the Λ moiety prefers to insert itself deeply into the minor groove while the Δ moiety, in the major groove, is somewhat displaced from the center of the DNA helix. The preceding, metastable bound geometries are concluded to be in the major groove for calf thymus DNA, poly(dG-dC)$_2$, and poly(dI-dC)$_2$, with the Δ,Δ form displaying an angle of the bidppz bridge relative the DNA helix axis of about 50°, whereas the corresponding angles for the meso- and Λ,Λ-forms in calf thymus DNA are around 65°, suggesting an orientation in the groove more parallel to the bases. By contrast, in poly(dA-dT)$_2$ none of the stereoisomers exhibits any distinguishable initial groove binding mode, but all seem to bind by threading intercalation directly.

Introduction

The design of small molecules, for sequence-specific nucleic acid recognition in the search for novel chemotherapeutics, DNA-probes, or as sensitive diagnostic agents, has received increasing attention ever since the structure of double helical DNA was first revealed in the early 1950s.[1] In the search for compounds with strong DNA affinity and slow dissociation kinetics, properties considered crucial for antitumor applications,[2] numerous natural antibiotics and their structural analogues have been investigated. One possibility to obtain slow dissociation from DNA is to involve threading of bulky subunits through the core of the DNA. An example is the natural antibiotic nogalamycin, which threads one of its two bulky sugar moieties through the base-stack of DNA to end up in a final binding mode in which one sugar moiety is situated in each groove.[3−6] As a result of the sterically hindered threading, which is also believed to be associated with local transient melting[7] or elongation and unstacking of the DNA,[8] the DNA interaction kinetics of nogalamycin is very slow and sequence dependent; for example, dissociation 150 times faster from poly(dA-dT)$_2$ than from poly(dG-dC)$_2$ has been reported.[9,10] Altromycin B, an antitumor antibiotic of the pluramycin family, also intercalates into DNA via a threading mechanism to position its disaccharide entity in the minor groove and the epoxide in the major groove.[11−13] Another interesting DNA-threading complex, netropsin-amsacrine, is a synthetic hybrid built up of one subunit structurally similar to the minor groove binder netropsin and one subunit resembling the intercalating antileukemia drug, amsacrine.[14]

A novel class of DNA-threading compounds is represented by the ruthenium complex, [μ-C4(cpdppz)$_2$(phen)$_4$Ru$_2$]$^{4+}$ (**2** in Figure 1), which according to spectroscopic and kinetic evidence, binds by bis-intercalating the cpdppz moieties between base pairs, thus placing the ruthenium centra and the alkylamide linker in opposite grooves.[15,16] Interaction kinetic results support a threading mechanism in which the Ru(phen)$_2$ moieties, which are in fact bulkier than the subunits of any previously studied DNA-threading molecule, thread themselves through the core of the DNA rather than via a mechanism in which the covalent linker is slinging itself around dissociated base pairs.[16] The DNA binding of the parent monomer compound [Ru(phen)$_2$dppz]$^{2+}$ (**3** in Figure 1) and its bipy analogue, [Ru(bipy)$_2$dppz]$^{2+}$, have been studied in great detail due to their rich photophysical repertoire.[17−27] Both these compounds bind to DNA by intercalating the dppz moiety between the base pairs of DNA, placing the remaining parts in one of the grooves.[23,26−29] When intercalated between the base pairs, the aza nitrogens of the dppz moiety are protected from hydrogen bonding to water, which is believed to play a crucial role for the excited-state relaxation;[30,31] thereby the luminescence quantum yield increases by several orders of magnitude ($>10^4$) a phenomenon referred to as the "light-switch" effect.[17,21,32,33] In studies of the binding of **2** to DNA it has been suggested, based on the similar features of LD spectra and also similar, remarkable increases in

* To whom correspondence should be addressed. Tel: +46-(0)31-7723055. Fax: +46-(0)31−7723858. E-mail: lincoln@phc.chalmers.se.

10.1021/jp036302f CCC: $25.00
Published on Web 09/30/2003

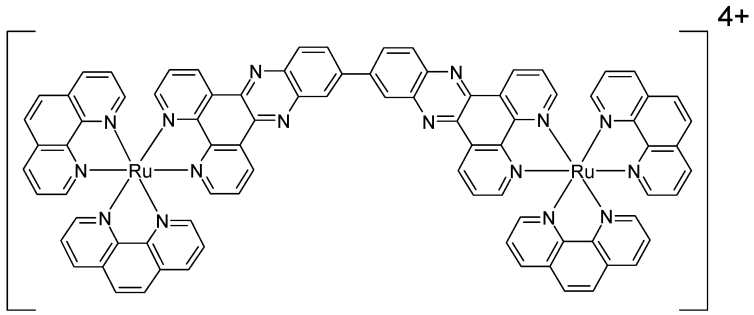

1

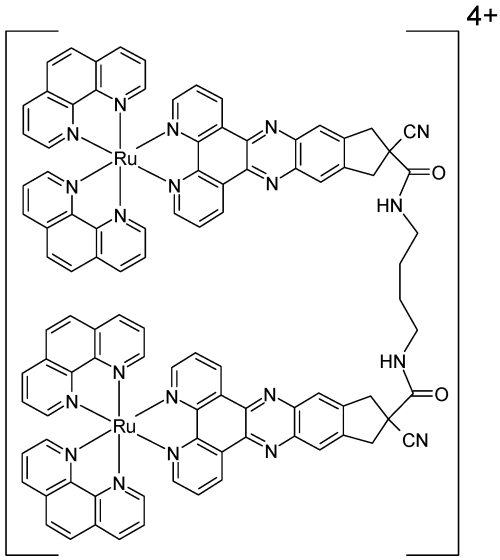

2

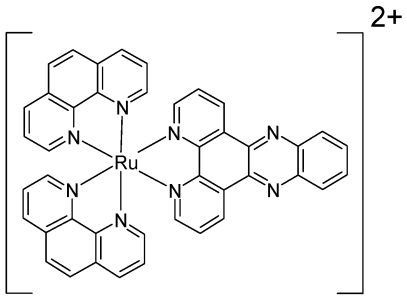

3

Figure 1. Ruthenium complexes. [μ-(11,11′-bidppz)(phen)$_4$Ru$_2$]$^{4+}$ (1), [μ−C4(cpdppz)$_2$(phen)$_4$Ru$_2$]$^{4+}$ (2), and [Ru(phen)$_2$dppz]$^{2+}$ (3); phen = 1,10-phenanthroline, 11,11′-bidppz = 11,11′-bis(dipyrido[3,2-*a*:2′,3′-*c*]phenazinyl), C4(cpdppz)$_2$ = *N*,*N*′ bis(cpdppz)-1,4-diaminobutane, cpdppz = 12-cyano-12,13-dihydro-11H-8-cyclopenta[b]dipyrido[3,2-*h*:2′,3′-*j*]phenazine-12-carbonyl, and dppz = dipyrido[3,2-*a*:2′,3′-*c*]phenazine.

fluorescence quantum yields, that each entity of this dimer binds to DNA almost identically to the monomer, **3**.[15]

Quite a different threading behavior has been recently observed for another novel dimeric ruthenium complex, [μ-(11,-11′-bidppz)(phen)$_4$Ru$_2$]$^{4+}$ (**1** in Figure 1), also studied because of its interesting electrochemical and photophysical properties,[34−36] and for which an early report suggested that both its enantiomeric Δ,Δ- and Λ,Λ-forms were bound to calf thymus (ct) DNA in one of the grooves rather than by intercalation between nucleobases.[37] Serendipitously, from a sample stored for several weeks at room temperature, it was later found that the groove-bound form of the Δ,Δ form was only a metastable state that is slowly reorganized into a final intercalative binding mode.[38] The rearrangement was found to occur faster (hours) at elevated temperature and at higher salt concentration, the kinetics monitored by an increase in fluorescence quantum yield or by a change in LD from a positive to a negative signal.[38] Additional evidence of the topologically different initial groove-bound and final intercalated geometries was enormous. Differences found in the SDS-induced dissociation kinetics, the dissociation of the initial groove binding, were effectively instantaneous, whereas the final, intercalated form needed several days at 45 °C to dissociate.[38] In the binding mode proposed for the final adduct, the bridging bidppz ligand is sandwiched between the bases in DNA with the two metal centers inevitably placed in opposite grooves. To dissociate from or to reach this binding geometry, the molecule would have to thread one of its bulky Ru(phen)$_2$ moieties through the DNA duplex in a similar way to that of **2**, for which, however, the flexible linker allows the metal centers to be in the same groove. However, we could not decide in which groove Δ,Δ-**1** is bound in its initial metastable state, whether it binds in a syn- or anti-conformation, or from which groove the complex is inserted when in the final intercalated geometry.

To throw light on the threading mechanism, we have used linear dichroism (LD), circular dichroism (CD), and fluorescence spectroscopy to probe the interactions of Δ,Δ-, meso-, and Λ,Λ-**1** with different types of DNA. In particular, we have utilized the meso form of **1** for probing which of the enantiomeric Ru(phen)$_2$dppz subunits of the dimer that preferentially binds to DNA by intercalating its dppz moiety deeply between the nucleobases and which enantiomeric part that has a preference for interacting with one of the grooves. The grooves are distinguished from each other by comparing the pairs {poly(dA-dT)$_2$, poly(dI-dC)$_2$} (similar minor grooves) and {poly(dG-dC)$_2$, poly(dI-dC)$_2$} (similar major grooves). We have found that the final binding geometry of the three stereoisomeric forms of **1** in ct-DNA, poly(dA-dT)$_2$, poly(dG-dC)$_2$, as well as in poly(dI-dC)$_2$, is in all cases characterized by the bridging bidppz ligand being sandwiched between the bases leaving one metal center in each groove, as has been proposed before for the Δ,Δ form in ct-DNA. We shall further conclude that the

initial metastable binding mode for Δ,Δ-**1** in ct-DNA, poly(dG-dC)$_2$, and poly(dI-dC)$_2$ is a predominantly major-groove-bound nonintercalated species, while meso- and Λ,Λ-**1** both display an initial metastable binding mode in ct-DNA that is more coplanar with the nucleoside bases but still nonthreading. We shall also present data in support of a more detailed final binding geometry for **1** in poly(dA-dT)$_2$, in which one dppz moiety is deeply intercalated from the minor groove, adopting an anti conformation relative to the other dppz moiety and deviating from coplanarity.

Materials and Methods

Chemicals. Calf thymus (ct) DNA, obtained from Sigma, was dissolved in buffer and filtered twice through a 0.8-μm Millipore filter before use. Polynucleotides were purchased from Pharmacia Biotech and used as obtained. All experiments were performed in aqueous buffers (100 mM NaCl, 1 mM cacodylate at pH 7.0 or 4 mM HEPES, 2 mM $MgCl_2$, 5 mM KCl at pH 7.4). The ruthenium stereoisomers were synthesized as described below.

Meso-1. A solution of 48 mg Λ-[Ru(phen)$_2$(1,10-phenanthroline-5,6-dione)](PF$_6$)$_2$[23] (0.05 mmol) in 2 mL of acetonitrile/water 1:1 was added dropwise with stirring to a solution of 100 mg 3,3′-diaminobenzidine tetrahydrochloride (0.25 mmol) and 82 mg sodium acetate (1 mmol) in 3 mL of acetic acid/acetonitrile/water 1:1:1. After 10 min, the crude product was precipitated by adding aqueous NH_4PF_6, collected on a filter and washed successively with water, absolute ethanol, diethyl ether and dried. Chromatography (neutral Al_2O_3 activity III, acetonitrile) gave first a small amount of the byproduct Λ,Λ-**1**, which after the desired mononuclear complex could be eluted with 10% ethanol in the same solvent. Evaporation to dryness gave 25 mg (44%) of Λ-[Ru(phen)$_2$(11-(3,4-diaminophenyl)-dipyrido[3,2-*a*:2′,3′-*c*]phenazine)](PF$_6$)$_2$, that was pure by TLC (silica gel, ethanol/5% aqueous NaBr 1:1). ES-MS (*m*/*e*, acetonitrile/water 1:1): 424.9 (100%). Calcd [M^{2+}] = 425.1; 994.8 (11%). Calcd [M $(PF_6)^+$] = 995.2.

The solid obtained above was redissolved in 2 mL of acetonitrile together with 29 mg of Δ-[Ru(phen)$_2$(1,10-phenanthroline-5,6-dione)](PF$_6$)$_2$ (0.03 mmol) and a few drops of acetic acid. After 30 min, TLC showed the reaction to be complete, and the product was precipitated by adding aqueous NH_4PF_6, collected on a filter, and washed successively with water, absolute ethanol, and diethyl ether and dried. Chromatography (neutral Al_2O_3 activity III, acetonitrile) gave 31 mg (87%) meso **1**, isolated as the chloride salt by precipitation of the fractions containing the product with (nBu)$_4$NCl in acetone.

Λ,Λ-1. A 48-mg sample of Λ-[Ru(phen)$_2$(1,10-phenanthroline-5,6-dione)](PF$_6$)$_2$ (0.05 mmol), 8 mg of 3,3′-diaminobenzidine tetrahydrochloride (0.02 mmol), and 7 mg of sodium acetate (0.08 mmol) were dissolved in 3 mL of acetic acid/acetonitrile/water 1:1:1. After standing at room temperature overnight, the crude product was precipitated by adding aqueous NH_4PF_6, collected on a filter and washed successively with water, absolute ethanol, and diethyl ether, and dried. Chromatography (neutral Al_2O_3 activity III, acetonitrile) gave 20 mg (60%) Λ,Λ-**1**, isolated as the chloride salt by precipitation of the fractions containing the product with (nBu)$_4$NCl in acetone. The Δ,Δ-enantiomer of **1** was prepared in the same way from Δ-[Ru(phen)$_2$(1,10-phenanthroline-5,6-dione)](PF$_6$)$_2$. ES-MS for **1**-(PF$_6$)$_4$ (*m*/*e*, acetonitrile/water 1:1): 371.5 (48%), calcd [M^{4+}] = 371.6; 543.8 (100%), calcd [M$(PF_6)^{3+}$] = 543.7; 887.6 (19%) calcd [M$(PF_6)_2^{2+}$] = 888.1. ^{1}H NMR for Δ,Δ-**1**-Cl_4 [δ (ppm), CD_3OD]: 7.78 (m, 2H), 7.83 (m, 3H), 7.92 (dd, 1H), 8.15 (m, 2H), 8.26 (m, 2H), 8.36 (d, 4H), 8.42 (ddd, 2H), 8.66 (d, 1H), 8.74 (m, 5H), 9.08 (d, 1H), 9.72 (dd, 1H), 9.82 (dd, 1H). UV−vis for **1**-Cl_4 [water, λ_{max}/nm, (ϵ/1000 $M^{-1}cm^{-1}$)]: 408 (74), 312 (108), 262 (192), 221 (146).

CD for Δ,Δ-**1**-Cl_4 [water, λ_{extr}/nm, ($\Delta\epsilon$/$M^{-1}cm^{-1}$)]: 467 (−37), 419 (+36), 297 (−197), 267 (−622), 256 (+340), 215 (+122). The CD signals for meso-**1** were less than 1% of the corresponding values for Λ,Λ-**1**.

Sample Preparation. Samples were prepared by mixing equal volumes of ruthenium complex and DNA dissolved in buffer. Unless otherwise stated, the sample concentrations were 10 μM Ru-complex and 160 μM DNA. Concentrations were determined on a Varian Cary 4B spectrophotometer. The extinction coefficients used were $\epsilon_{408\ nm} = 74000\ M^{-1}cm^{-1}$ for [μ-(11,11′-bidppz)(phen)$_4$Ru$_2$]$^{4+}$,[39] $\epsilon_{260\ nm} = 6600\ M^{-1}cm^{-1}$ for ct-DNA, $\epsilon_{262\ nm} = 6600\ M^{-1}cm^{-1}$ for poly(dA-dT)$_2$, $\epsilon_{254\ nm} = 8400\ M^{-1}cm^{-1}$ for poly(dI-dC)$_2$, and $\epsilon_{258\ nm} = 6900\ M^{-1}cm^{-1}$ for poly(dG-dC)$_2$.

Flow Linear Dichroism. Linear dichroism[40] is defined as the difference in absorbance of linearly polarized light parallel and perpendicular to a macroscopic orientation axis (here the flow direction)

$$LD(\lambda) = A_{II}(\lambda) - A_{\perp}(\lambda) \tag{1}$$

The reduced linear dichroism LD^r is calculated as

$$LD^r(\lambda) = LD(\lambda)/A_{iso} \tag{2}$$

where A_{iso} represents the absorbance of the same isotropic sample. The LD^r of a single electronic transition, *i*, in a uniaxially oriented sample can be written as

$$LD^r_i = \frac{3}{2}S(3\cos^2\alpha_i - 1) \tag{3}$$

where α_i is the angle between the transition moment and the molecular orientation axis, in this case the DNA helix axis. Samples with ruthenium complex and DNA were oriented in a Couette flow cell with an outer rotating cylinder at a shear gradient of 3000 s^{-1}. LD spectra were measured on a Jasco J-720 CD spectropolarimeter equipped with an Oxley prism to obtain linearly polarized light. All spectra were recorded between 220 and 650 nm and baseline-corrected by subtracting the spectrum recorded for the nonoriented sample.

Circular Dichroism. Circular dichroism (CD) is defined as the difference in absorbance of left and right circularly polarized light. CD spectra were measured on a Jasco J-720 spectropolarimeter using a 4 mm quartz cell. All spectra were recorded between 220 and 650 nm and corrected for background contributions.

Steady-State Luminescence. Emission spectra were recorded on a xenon-lamp-equipped SPEX fluorolog τ-2 spectrofluorimeter (JY Horiba) between 420 and 800 nm using an excitation wavelength of 415 nm. Time-based association and dissociation measurements were performed on a SPEX fluorolog τ-3 spectrofluorimeter (JY Horiba) setting the excitation wavelength to 420 nm and the emission wavelength to 630 nm.

Luminescence Lifetimes. Lifetime measurements were performed on a SPEX fluorolog τ-2 spectrofluorimeter using the phase modulation technique,[41] setting the excitation wavelength to 415 nm, and using a 550 nm cutoff filter in the emission channel. Lifetimes were obtained from spectral data using a program written for the MatLab software.

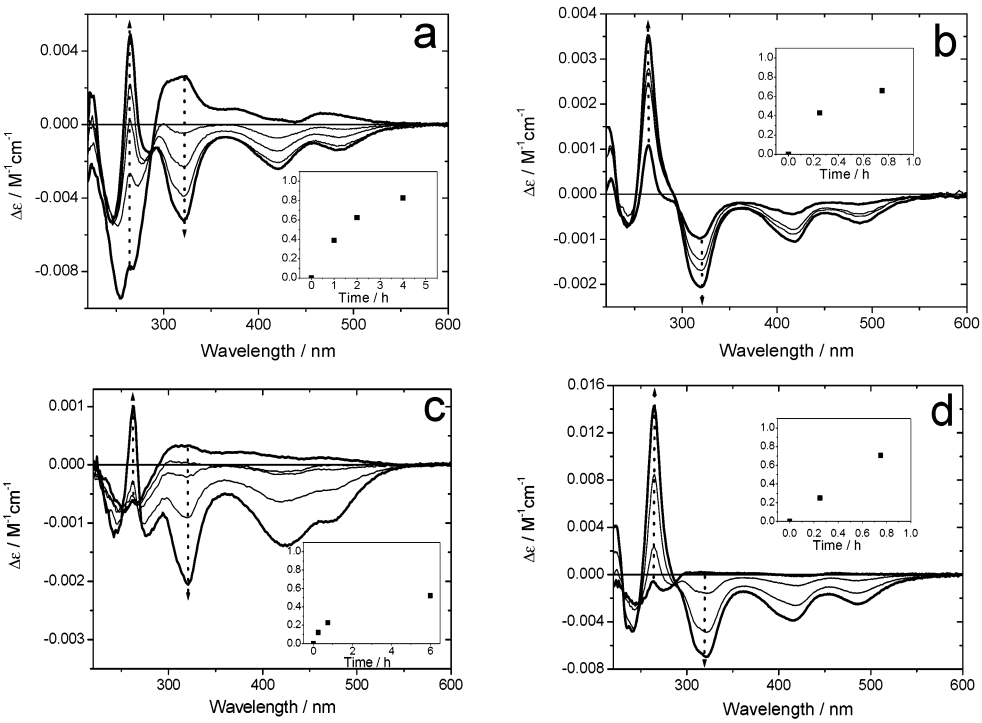

Figure 2. Flow linear dichroism spectra of 10 μM Δ,Δ-**1** and 160 μM of different DNAs (P/Ru-ratio of 8) at various times after mixing (100 mM Na^+, 1 mM sodium cacodylate, pH 7). (a) Δ,Δ-**1** and ct-DNA (0, 1, 2, 4, and 16 h at 45 °C), (b) Δ,Δ-**1** and poly(dA-dT)$_2$ (0, 15, 45 min at room temperature and overnight at 45 °C), (c) Δ,Δ-**1** and poly(dG-dC)$_2$ (0, 15, 45, and 360 min at room temperature and overnight at 45 °C), and (d) Δ,Δ-**1** and poly(dI-dC)$_2$ (0, 15, and 45 min at room temperature and overnight at 45 °C). The thick-line spectra are the start and final ones and the arrows specify spectral change with time. The arrows at 320 nm indicate the change at the wavelength where the long-axis polarized transition moment of the bidppz ligand is dominating, and the arrows around 260 nm mark changes where the transition of the phenanthroline-ligands makes the largest contribution. Insets: $(LD_0 - LD(t))/(LD_0 - LD_{final})$, calculated at 320 nm, vs time showing the progress of the reactions.

Results

Figure 2 shows the time evolution of flow linear dichroism (LD) spectra of Δ,Δ-**1** in the presence of different DNAs: ct-DNA (a), poly(dA-dT)$_2$ (b), poly(dG-dC)$_2$ (c), and poly(dI-dC)$_2$ (d). With ct-DNA (Figure 2a), the change in linear dichroism above 300 nm from positive to negative, takes almost 1 day at elevated temperature (45 °C) and high salt concentration (100 mM Na^+). This indicates a major change in binding geometry and, as concluded in a previous study,[38] the slow rearrangement and change in LD are due to a change from an initial groove-bound to a final intercalated geometry. By contrast, the interaction between Δ,Δ-**1** and poly(dA-dT)$_2$ is lacking the positive linear dichroism at short times (Figure 2b). Comparing the kinetics in the insets of Figure 2b and Figure 2a, it is evident that although Figure 2a refers to an elevated temperature (45 °C), the reaction of Δ,Δ-**1** is still significantly slower with ct-DNA than with poly(dA-dT)$_2$. In poly(dA-dT)$_2$, Δ,Δ-**1** reaches its final intercalative binding geometry much more rapidly and any groove-bound intermediate cannot be discriminated within the time resolution of LD after mixing.

In Figure 2c, the linear dichroism spectra of Δ,Δ-**1** and poly(dG-dC)$_2$ under the same conditions as in Figure 2b are shown. It is clear that the positive component of the LD spectrum seen in Figure 2a is present also for poly(dG-dC)$_2$. However, the rearrangement (i.e., change from positive to negative LD) is remarkably faster in poly(dG-dC)$_2$ than that in ct-DNA, regarding that the latter measurements were performed at 45 °C while the former were at room temperature. Figure 2d shows the same experiment performed in poly(dI-dC)$_2$. The instantaneous binding of Δ,Δ-**1** to poly(dI-dC)$_2$ results in a weakly positive linear dichroism resembling the observations in ct-DNA and poly(dG-dC)$_2$, which after 15 min becomes all negative above 300 nm, closely resembling the spectrum measured immediately after mixing Δ,Δ-**1** and poly(dA-dT)$_2$. In conclusion, the same kind of spectral evolution is observed for ct-DNA, poly(dG-dC)$_2$, and poly(dI-dC)$_2$. However, as can be seen in the insets of Figure 2, there are great differences in the rates of transformation, where the change in linear dichroism for Δ,Δ-**1** is by far the slowest in ct-DNA followed by poly(dG-dC)$_2$ and poly(dI-dC)$_2$.

Figure 3 shows the linear dichroism spectra corresponding to the final binding geometries of the Δ,Δ-, meso-, and Λ,Λ-**1** complexes with ct-DNA (Figure 3a), poly(dA-dT)$_2$ (Figure 3b), poly(dG-dC)$_2$ (Figure 3c), and poly(dI-dC)$_2$ (Figure 3d), obtained after incubation at 50 °C overnight. Due to problems arising from aggregation and condensation of DNA strands when adding meso-, and Λ,Λ-**1** to some of the DNAs in sodium cacodylate-buffer, a magnesium HEPES buffer was used instead. Replacing the monovalent sodium (100 mM) in the cacodylate-buffer with a low concentration of the divalent magnesium (2 mM) in the HEPES-buffer caused an increase by approximately a factor of 2 in the binding rate. To facilitate detection of spectral variations between the DNA-bound isomeric ruthenium complexes, the spectra for each DNA were normalized to the same LD value as Λ,Λ-**1** for the negative peak at ~320 nm. The main features of the linear dichroism spectra above 300 nm are basically the same, the spectra being all negative and with similar shapes. This suggests that the final binding mode is basically the same for all three stereoisomers and independent of the kind of DNA. Referring to our previous study and conclusion that Δ,Δ-**1** is intercalated in ct-DNA,[38] the spectral similarities suggest effectively the same final intercalative DNA-binding geometry in all cases. The distinct difference between

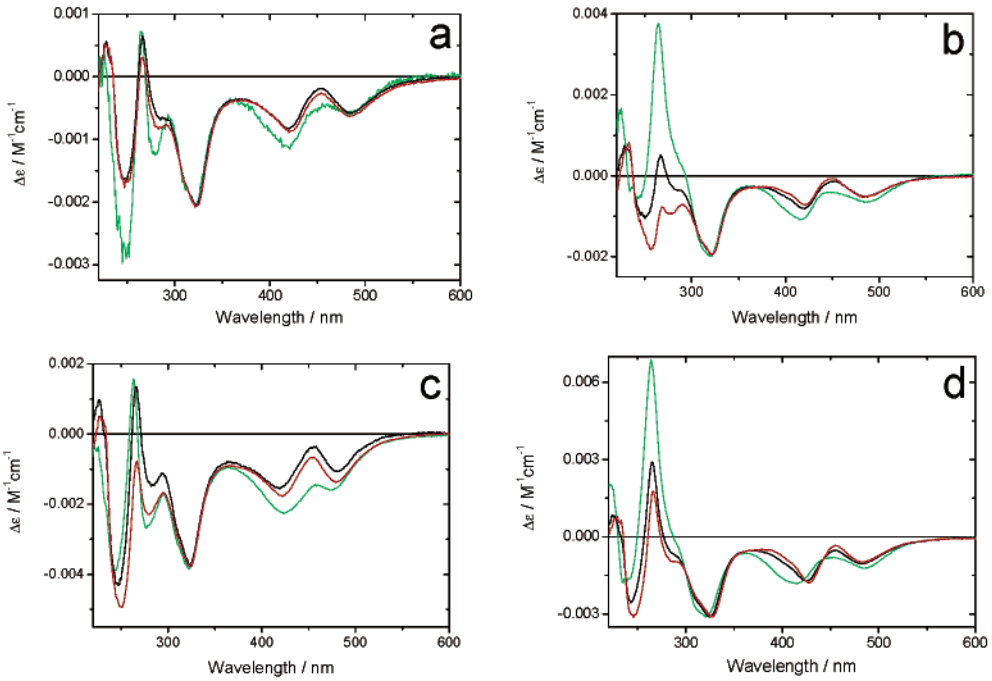

Figure 3. Flow linear dichroism spectra of 10 μM Δ,Δ (green curve), meso (black curve), and Λ,Λ (red curve) forms of **1** in the presence of 160 μM of different DNAs (P/Ru-ratio of 8): (a) ct-DNA, (b) poly(dA-dT)$_2$, (c) poly(dG-dC)$_2$, and (d) poly(dI-dC)$_2$. (Measurements made at room temperature in 4 mM HEPES, 2 mM $MgCl_2$, and 5 mM KCl, pH 7.4).

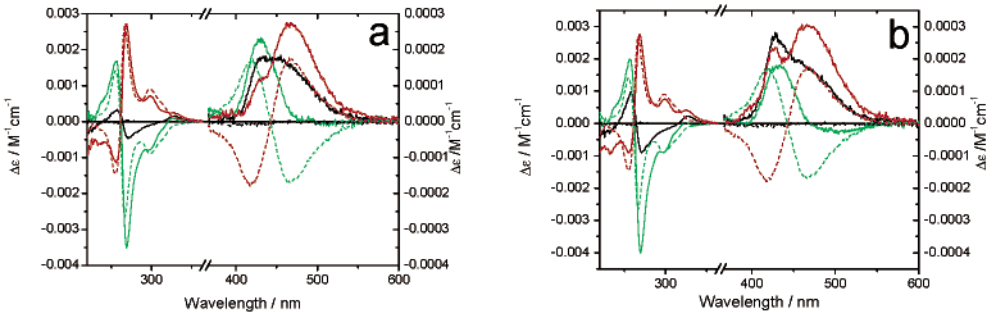

Figure 4. Circular dichroism spectra of 10 μM Δ,Δ- (green curve), meso- (black curve), and Λ,Λ-**1** (red curve) in the presence of 160 μM of (a) ct-DNA and (b) poly(dA-dT)$_2$ (P/Ru-ratio of 8). Spectra corrected for inherent CD of DNA. Included for comparison are also CD spectra of 10 μM Δ,Δ- (green dashed curve), meso- (black dashed curve), and Λ,Λ-**1** (red dashed curve) free in buffer. Note that the long-wavelength parts of the spectra have been multiplied by 10 (scale to the right). Experimental conditions otherwise as in Figure 3.

Δ,Δ- and Λ,Λ-**1** seen in the LD spectrum at 400−500 nm (Figure 3a and b), can be explained by the antisymmetric orientational arrangement of transition moments of opposite enantiomers of **3** when intercalated into DNA, in combination with a small clockwise roll of the short axis of the intercalated dppz moiety by some 10°. We shall return to these structural variations in the Discussion. Another interesting feature in this "roll region" is that the LD spectra of meso-**1** bound to the four different DNAs are more similar to the spectra of Λ,Λ-**1** than to those of Δ,Δ-**1**, suggesting that it is the Λ moiety of the meso form, and not the Δ moiety, that is intercalated.

Considerable variations in LD spectra can be seen in Figure 3, parts b and d between the three stereoisomeric forms around 260 nm. In poly(dA-dT)$_2$ (Figure 3b), the Δ,Δ-form shows a strong positive LD peak, whereas the meso- and Λ,Λ-forms only show a small positive and a small negative LD peak, respectively. In this region of the spectrum, strong absorption intensity originates from excitonic coupling of long-axis polarized intra-ligand transitions of the phenanthroline moieties ($B(A_2)$ in **3**). The substantial differences between the stereoisomeric forms in this region of the linear dichroism spectra suggest that there are considerable variations in the orientation of the phenanthroline ligands. A similar pattern as is observed for poly(dA-dT)$_2$ can also be seen for the isomers bound to poly(dI-dC)$_2$ (Figure 3d), although certain differences in LD shapes and amplitudes indicate that there could be some structural variations between the polynucleotides. For example, when bound to poly(dI-dC)$_2$ the Λ,Λ form shows a positive LD around 260 nm, where the absorption is dominated by the phenanthroline transitions. Figure 3c shows that Δ,Δ- and meso-**1** bound to poly(dG-dC)$_2$ both show resemblance with the spectra for the three stereoisomers bound to ct-DNA (Figure 3a), whereas when bound to poly(dG-dC)$_2$, Λ,Λ-**1** shows a less positive LD peak in this wavelength region.

Figure 4 shows circular dichroism (CD) spectra of the Δ,Δ-, meso-, and Λ,Λ-**1** complexes, free as well as in their final binding modes with ct-DNA (Figure 4a) and poly(dA-dT)$_2$ (Figure 4b). The strong phenanthroline exciton CD couplet centered at 260 nm is positive at high energy and negative at low energy for Δ,Δ-**1** just as with Δ-**3**.[42] The CD profile for Δ,Δ-**1** in the visible part of the spectrum shows a positive peak at 420 nm and a negative peak of about equal amplitude at 465 nm.

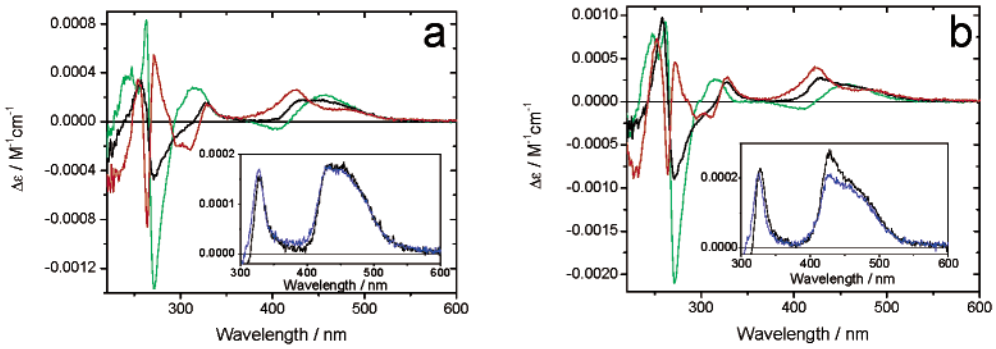

Figure 5. Differential circular dichroism spectra ($CD_{DNA-bound}$-CD_{free}) of 10 μM Δ,Δ- (green curve), meso- (black curve), and Λ,Λ-**1** (red curve) in the presence of 160 μM DNA (P/Ru-ratio of 8): (a) ct-DNA, (b) poly(dA-dT)$_2$. Otherwise, as in Figure 3. Insets: Calculated average ($CD_{\Delta,\Delta}$ + $CD_{\Lambda,\Lambda}$)/2 (blue curve), compared to differential circular dichroism of meso-**1** (black curve) bound to various DNAs.

TABLE 1: Luminescence Properties of Δ,Δ-, Meso-, and Λ,Λ-1 in the Presence of Various Types of DNA (P/Ru Ratio of 8)

	calf thymus DNA				poly(dA-dT)$_2$		
	ϕ^a	$\tau_1{}^b$/ns	τ_2/ns	τ_3/ns	ϕ	τ_1/ns	τ_2/ns
Δ,Δ	0.02	390 (0.17)	184 (0.35)	44 (0.48)	0.09	626 (0.84)	118 (0.16)
meso	0.009	439 (0.042)	128 (0.46)	37 (0.50)	0.013	224 (0.20)	72 (0.80)
Λ,Λ	0.007	382 (0.030)	120 (0.38)	37 (0.59)	0.011	169 (0.32)	59 (0.68)
	poly(dG-dC)$_2$				poly(dI-dC)$_2$		
	ϕ	τ_1/ns	τ_2/ns	τ_3/ns	ϕ	τ_1/ns	τ_2/ns
Δ,Δ	0.003	679 (0.021)	118 (0.10)	18 (0.87)	0.097	617 (0.79)	137 (0.21)
meso	0.005	588 (0.074)	142 (0.34)	17 (0.58)	0.011	272 (0.12)	67 (0.88)
Λ,Λ^c	0.003	680 (0.091)	146 (0.18)	14 (0.73)	0.016	383 (0.36)	112 (0.64)

[a] Luminescence quantum yield. [b] Excited-state lifetimes (τ), and in parentheses, normalized preexponential factors reflecting mole fractions of the different luminescing species at $t = 0$ (directly after illumination). [c] Due to low emission, τ_1 was fixed, but the other lifetimes and all three preexponential factors were allowed to vary.

Figure 5 shows differential CD ($CD_{diff} = CD_{DNA-bound} - CD_{free}$) spectra of the Δ,Δ-, meso-, and Λ,Λ-**1** complexes with regard to their final binding modes in ct-DNA (Figure 5a) and poly(dA-dT)$_2$ (Figure 5b).[43,44] In both ct-DNA and poly(dA-dT)$_2$, the differential CD of the UV region is dominated by the phenanthroline exciton (Figure 5a and b) and the differential CD of Δ,Δ-**1** exhibits a larger amplitude than those of the other stereoisomers. This is also the case when **1** is bound to poly(dG-dC)$_2$ and poly(dI-dC)$_2$ (Supporting Information S2). We note that the Δ,Δ- and meso-forms have very similar shapes of differential CD in the UV region. In the visible wavelength region, the differential CD signals in ct-DNA, poly(dA-dT)$_2$, poly(dG-dC)$_2$, and poly(dI-dC)$_2$ are similar to each other, all stereoisomers exhibiting predominantly positive features, except a small negative peak on the blue side for Δ,Δ-**1**. Furthermore, the CD of the initial state of **1** in ct-DNA is very little perturbed compared to that of the free **1** (data not shown), although we know from LD that the angle between **1** and the DNA helix axis is different in the three stereoisomers. It is also worth mentioning that the differential CD in ct-DNA is approximately 2.5 times larger per ruthenium for **1** than for **3** (Supporting Information S1), and a comparison shows that the effect, a positive increase in the CD, coincides with the positions of the strong bidppz long-axis polarized transitions at 320 and 410 nm as well as the lowest MLCT band at 460 nm.

The insets in Figure 5 compare the measured differential CD for the actual meso-form and the calculated average "meso-spectrum" (($CD_{\Delta,\Delta}$+$CD_{\Lambda,\Lambda}$)/2) for each of the DNAs. There is a remarkable agreement between the measured and this calculated meso-spectra in ct-DNA. This long-wavelength part of the spectrum is mainly a result of d $\rightarrow \pi^*$ metal-to-ligand charge transfer (MLCT) transitions together with the intra-ligand transition of the bidppz moiety, and any extra CD could hence reflect a chiral conformation due to a preferred rotation around the central pivot bond. The similar differential CD effects thus suggest that the chiral conformation of the bidppz ligand (i.e., the dihedral angle relative to the central inter-nuclear bond) is essentially the same in the three stereoisomers. The agreement is also good in poly(dA-dT)$_2$ (Inset, Figure 5b) and poly(dI-dC)$_2$ (Supporting Information S2), but only fair in poly(dG-dC)$_2$ (Supporting Information S2).

Table 1 presents luminescence quantum yields (ϕ) and lifetimes of the final binding states of Δ,Δ-, meso-, and Λ,Λ-**1** in ct-DNA, poly(dA-dT)$_2$, poly(dG-dC)$_2$, and poly(dI-dC)$_2$ measured in a 4 mM HEPES-buffer (2 mM $MgCl_2$ and 5 mM KCl, pH 7.4). As can be seen in the table, the luminescence quantum yields are similar in poly(dA-dT)$_2$ and poly(dI-dC)$_2$. The quantum yields of Δ,Δ-**1** bound to those polynucleotides are considerably higher ($\phi \sim 0.10$) than those for the other two stereoisomers ($\phi \approx 0.015$). Although the quantum yields in ct-DNA show the same trend (i.e., Δ,Δ-**1** has somewhat higher quantum yield ($\phi = 0.02$) than the two other stereoisomers ($\phi \approx 0.01$)) the difference is here much less pronounced. The final binding mode in poly(dG-dC)$_2$ shows by far the lowest quantum yields ($\phi \approx 0.005$) for all three stereoisomers. The agreement of luminescence lifetimes as well as preexponential factors (α, corresponding to mole fractions) between the luminescent species of Δ,Δ-**1** in poly(dA-dT)$_2$ and poly(dI-dC)$_2$ is almost perfect, as expected with very similar final binding geometries in these two polynucleotides. This is also true for meso-**1** in poly(dA-dT)$_2$ and poly(dI-dC)$_2$. However, Λ,Λ-**1** displays significant differences in its luminescence lifetimes between poly(dA-dT)$_2$ and poly(dI-dC)$_2$.

A low effective luminescence quantum yield of **1** in poly(dG-dC)$_2$ is also reflected in the luminescence lifetimes and preexponential factors of the different excited species: the

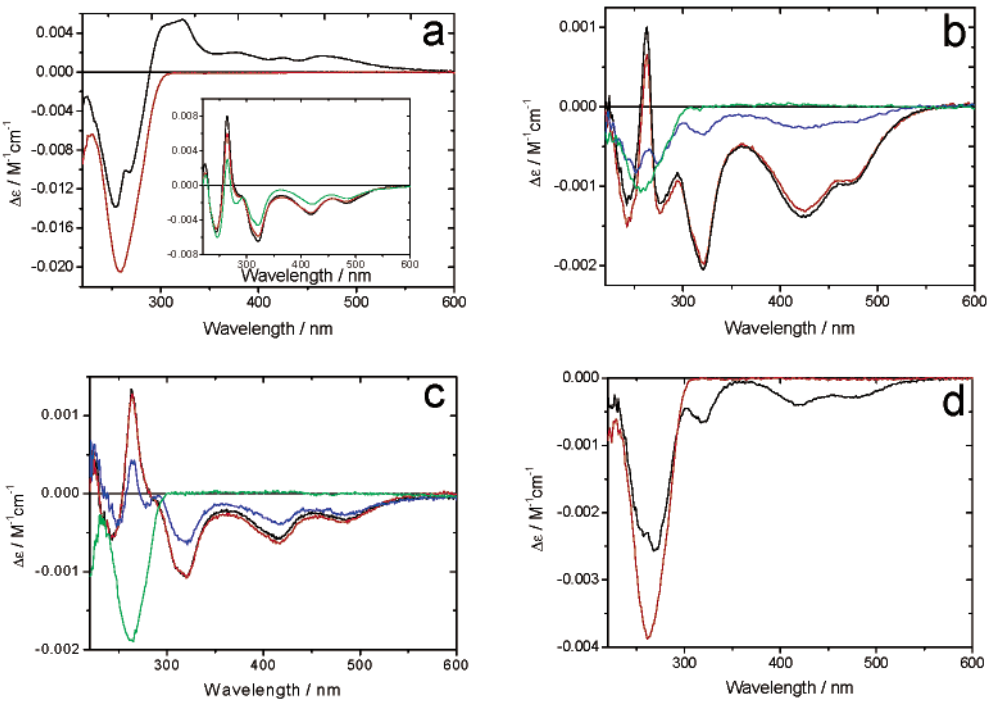

Figure 6. Dissociation from DNA at different times after incubation with metal complex. (a) 160 μM calf thymus DNA mixed with 10 μM Δ,Δ-**1** (P/Ru-ratio of 8). LD spectra recorded immediately after mixing (black curve) and subsequent addition of 0.6% SDS (red curve). Inset (a): LD spectra recorded after preequilibration overnight at 50 °C (black curve), subsequent addition of 0.6% SDS (red curve), and after 24 h of incubation at 45 °C following addition of 0.6% SDS (green curve). (b) 160 μM poly(dG-dC)$_2$ mixed with 10 μM Δ,Δ-**1**. As inset of (a) but with an LD spectrum 1 h after SDS (0.6%) addition also included (blue curve). (c) 160 μM poly(dA-dT)$_2$ mixed with 10 μM Δ,Δ-**1**. As (a) but with LD spectra 2 h (blue curve) and 24 h (green curve) after SDS (0.6%) addition at 45 °C. (d) 160 μM calf thymus DNA mixed with 10 μM Λ,Λ-**1**. Otherwise, as in (a).

species with the shortest luminescent lifetime (10−20 ns) dominates the emission in all three stereoisomers. It could also be noted that τ_2 of meso-**1** has a significantly higher preexponential factor than the two enantiomers, which is also born out as a very small quantum yield. The luminescence lifetimes and preexponential factors of **1** in ct-DNA show notable similarities for the meso- and Λ,Λ-forms. However, a higher molar fraction of the longest lifetime and also a considerable enhancement in τ_2 can be observed for Δ,Δ-**1**. The lifetimes measured for **1** in ct-DNA are between those found for poly(dA-dT)$_2$ and poly(dG-dC)$_2$, though the data could not be fitted by a hypothetical combination of pure poly(dA-dT)$_2$ and poly(dG-dC)$_2$ lifetimes.

In Figure 6, SDS-sequestered dissociation of Δ,Δ-**1** from ct-DNA (a), poly(dG-dC)$_2$ (b), poly(dA-dT)$_2$ (c), and Λ,Λ-**1** from ct-DNA (d) is studied. Figure 6a shows dissociation of the initial metastable binding mode of Δ,Δ-**1** in ct-DNA. Virtually immediately after addition of SDS, the complex dissociates from DNA (red curve, Figure 6a). By contrast, the dissociation of Δ,Δ-**1** from ct-DNA in the final, intercalative binding mode is extremely slow (Inset, Figure 6a). Figure 6b shows the SDS-sequestered dissociation of Δ,Δ-**1** from the final binding state in poly(dG-dC)$_2$. Also in this case, the dissociation is very slow (red, blue, and green curve, Figure 6b). Figure 6c shows LD spectra measured immediately after mixing poly(dA-dT)$_2$ and Δ,Δ-**1** and after addition of SDS. In contrast to the measurements performed on the initial binding mode of ct-DNA, the dissociation is now extremely slow (red, blue, and green curve, Figure 6c). Figure 6d shows the fast dissociation of Λ,Λ-**1** when in its initial metastable binding mode in ct-DNA.

Discussion

We previously reported a remarkably slow reorganization from an initial groove-bound to a final intercalated geometry of Δ,Δ-**1** upon interaction with ct-DNA and poly(dA-dT)$_2$.[38] The slowness of the rearrangement as well as subsequent dissociation suggested that the complex has to thread itself through the double helical DNA to reach its final binding state. High activation energies for both rearrangement and dissociation were also in accord with an associated profound structural change, such as one involving at least one base-pair opening.

Final Intercalative Binding Mode. One of the key observations in this study is that the LD spectra of the three forms of **1** in the various DNAs at equilibrium show great resemblance with the spectrum for Δ,Δ-**1** in ct-DNA (Figure 3). In particular, this holds for the series of negative bands above 300 nm. From the reduced linear dichroism, LD^r, of the negative LD band at 320 nm, we have estimated the angle between the bidppz ligand long-axis of Δ,Δ-**1** and the DNA helix axis in ct-DNA to be about 70°.[38] Although deviating from 90°, this result appears still consistent with intercalation of one of the dppz moieties, because both of them do not have to be aligned parallel with the DNA bases. The similar LD bands at 320 nm seen in Figure 3, and similar LD^r magnitudes, thus suggest that all three isomers of **1** bind by intercalation to all of the DNAs in their final binding geometries. That the final binding geometries are basically the same, the bidppz ligand stacked between the DNA bases, is also indicated by the differential CD spectra shown in Figure 5, in which the average of Δ,Δ- and Λ,Λ-**1** have nearly the same shapes as meso-**1** regardless of type of DNA.

Further support for a final intercalative binding mode of **1** in ct-DNA, poly(dA-dT)$_2$, and poly(dI-dC)$_2$ are the luminescence quantum yields and time-resolved luminescence data given in Table 1. As mentioned above, the parent monomer compound, [Ru(phen)$_2$dppz]$^{2+}$, exhibits an enormous increase in luminescence quantum yield upon intercalation of the dppz ligand into the DNA base stack.[17] Similar high quantum yield and

resemblance of luminescence lifetimes have been observed for Δ,Δ-**1** bound to poly(dA-dT)$_2$.[38] The agreement between quantum yields, lifetimes, and preexponential factors of Δ,Δ-**1** when bound to poly(dI-dC)$_2$ and those in poly(dA-dT)$_2$ is remarkable (Table 1) and suggests that also finer details of the intercalating geometries in the two polynucleotides are very similar. Studying the luminescence properties of meso- and Λ,Λ-**1** in poly(dA-dT)$_2$ and poly(dI-dC)$_2$, it is obvious that the lifetimes are shorter and the quantum yields lower, than for the Δ,Δ-form. This effect is not unexpected, and a similar variation has been observed for Λ- compared to Δ-[Ru(phen)$_2$dppz]$^{2+}$ when intercalated into poly(dA-dT)$_2$,[28] but it again indicates the predominance of the Λ over the Δ moiety of the meso isomer upon interaction with the DNA. The quantum yield of Δ,Δ-**1** ($\phi = 0.02$) when intercalating into ct-DNA is approximately 1500 times greater than that in water solution.

The luminescence properties of **1** in poly(dG-dC)$_2$ given in Table 1 show dominating large preexponential factors ($\alpha = 0.58-0.87$) for a lifetime ($\tau_3 = 14-18$ ns) that is significantly shorter than any lifetime found in the other DNAs. As a result, the quantum yields are much lower in poly(dG-dC)$_2$ than in for example poly(dA-dT)$_2$ (Δ,Δ-**1** differs by a factor of 30). Although the difference in quantum yields in poly(dG-dC)$_2$ and ct-DNA is large, it could still be established that the final binding mode of **1** in poly(dG-dC)$_2$ is indeed an intercalated one: when studying the SDS-sequestered dissociation from the final binding mode of Δ,Δ-**1** in ct-DNA and poly(dG-dC)$_2$, we find that 30% of the complex dissociates from the ct-DNA after 24 h of incubation at 45 °C (Inset, Figure 6a) while as much as 80% of the complex dissociates from poly(dG-dC)$_2$ 1 h after addition of SDS. Although the dissociation process is faster in poly(dG-dC)$_2$ than in ct-DNA, it is still very slow compared to the instantaneous dissociation observed for the initial binding mode in ct-DNA (Figure 6a), as expected if this initial mode is a groove bound one (vide infra). This suggests that one of the bulky Ru(phen)$_2$ moieties of Δ,Δ-**1** is threaded through the DNA also in poly(dG-dC)$_2$ and thus has to be intercalated in its final DNA-binding geometry.

Initial Binding Modes are in Major Groove. Previously, we have shown that Δ,Δ-**1** initially binds in one of the grooves of ct-DNA, based on the positive LD, low luminescence, and the immediate dissociation from the first binding mode (also evidenced from Figure 6a).[38] Also when Δ,Δ-**1** binds to poly(dG-dC)$_2$, and poly(dI-dC)$_2$, the initial LD signal above 300 nm is positive (Figure 2). By contrast, no initial positive LD can be detected above 300 nm when Δ,Δ-**1** is mixed with poly(dA-dT)$_2$. Furthermore, the dissociation from the immediately formed complex between Δ,Δ-**1** and poly(dA-dT)$_2$ is extremely slow (Figure 6c), suggesting that Δ,Δ-**1** gets directly threading-intercalated, virtually without passing through an intermediate groove-bound state. The positive LD for the first interaction between Δ,Δ-**1** and ct-DNA, poly(dG-dC)$_2$, and poly(dI-dC)$_2$ demonstrate that the angle between the DNA helix axis and the bidppz ligand in Δ,Δ-**1** is less than the magic angle, 54.7° (eq 3). The measurements on the shorter polynucleotides, poly(dI-dC)$_2$ and poly(dG-dC)$_2$, displaying a worse flow orientation than ct-DNA, did not allow a fast enough recording to quantitatively reveal the maximum positive LD amplitude. Therefore, the angle between the DNA helix axis and the bidppz ligand in Δ,Δ-**1** for the initial binding mode was calculated using the LD^r value obtained with ct-DNA at 320 nm, giving 48° and thus suggesting a groove bound geometry, possibly in the minor groove. However, the great differences of the minor grooves of poly(dI-dC)$_2$ and poly(dG-dC)$_2$, together with the similar positive LD signals, contradict that Δ,Δ-**1** binds in the minor groove. Instead, we suggest that the complex binds in the chemically similar major grooves of poly(dG-dC)$_2$ and poly(dI-dC)$_2$. Also, the estimated angle around 50° is consistent with an initial major groove bound geometry in these polynucleotides. The result with ct-DNA containing guanine-cytosine base pairs as well is also consistent with major groove binding.

Previously, Λ,Λ-**1** was found to bind to ct-DNA initially at an angle between the bidppz ligand and the DNA helix axis of 64°,[37] thus approaching the angle of 70° obtained for the final, threading binding geometry. However, despite similar angles, there is a significant difference when studying the dissociation: from this initial binding mode, Λ,Λ-**1** dissociates instantaneously (Figure 6d). This implies that the initial binding mode is nonthreaded, but nevertheless must have a geometry where its bidppz ligand is more or less perpendicular to the DNA helix axis. This is in conflict with any arrangement in the minor groove. Therefore, we propose that the initial binding mode of Λ,Λ-**1** in ct-DNA is in the major groove, where it might be stabilized by quasi-intercalation[45,46] of the bidppz moiety in a *syn*-conformation, leaving the positively charged ruthenium centra close to the backbones of the DNA. Studying the dissociation of meso-**1** from its initial binding mode, a binding geometry resulting in a similar LD spectrum as that for the Λ,Λ-form (data not shown), we could verify that also meso-**1** instantaneously leaves ct-DNA (data not shown). Along the same line of reasoning, it may therefore be argued that meso-**1** is also initially bound in the major groove.

Detailed Final Binding Geometry. The final intercalative binding geometry, where parts of the bidppz ligand are stacked between the DNA bases, places one metal center in the minor groove and one in the major groove. It is relevant to discuss the degree of rotation around the central pivot bond of the bidppz ligand, which determines the relative orientations of the two Ru(phen)$_2$ moieties in the grooves, the position of the bidppz ligand, and which Ru(phen)$_2$ moiety has its dppz positioned in the base stack. Referring to the final binding geometry of **1** in poly(dA-dT)$_2$, schematically visualized in Figure 7, we shall discuss similarities and differences vis-a-vis other final binding geometries.

To be able to deduce a detailed binding geometry, we first need to establish whether the complex has one of its [Ru(phen)$_2$dppz] subunits more deeply intercalated (asymmetric case) or has a centered type of intercalation (symmetric case). The former geometry, with one of the positively charged ruthenium centra closer to the negatively charged phosphate groups, is expected to be more favorable than a symmetric arrangement (Figure 7). Furthermore, upon excitation, one of the rutheniums of **1** will be formally oxidized, giving it an extra positive charge, which will be energetically most favorable for the ruthenium closest to the backbone phosphates (i.e., the one corresponding to the more deeply intercalated dppz moiety). The transfer of an electron will occur to the dppz moiety closest to the initially excited ruthenium. This explains the great similarities in luminescence properties between **1** (Table 1) and its monomer counterpart (**3**) when bound to poly(dA-dT)$_2$, supporting that their luminescing entities are essentially the same and are bound in a similar manner.

The remarkable similarity in LD between meso- and Λ,Λ-**1** bound to poly(dA-dT)$_2$ (Figure 3b) suggests that also meso-**1** prefers to intercalate its Λ part deeply. This conclusion is supported by the similarities in luminescence properties of meso- and Λ,Λ-**1** bound to poly(dA-dT)$_2$. Assuming that the Λ part of meso-**1** is deeply intercalated, the difference in LD below

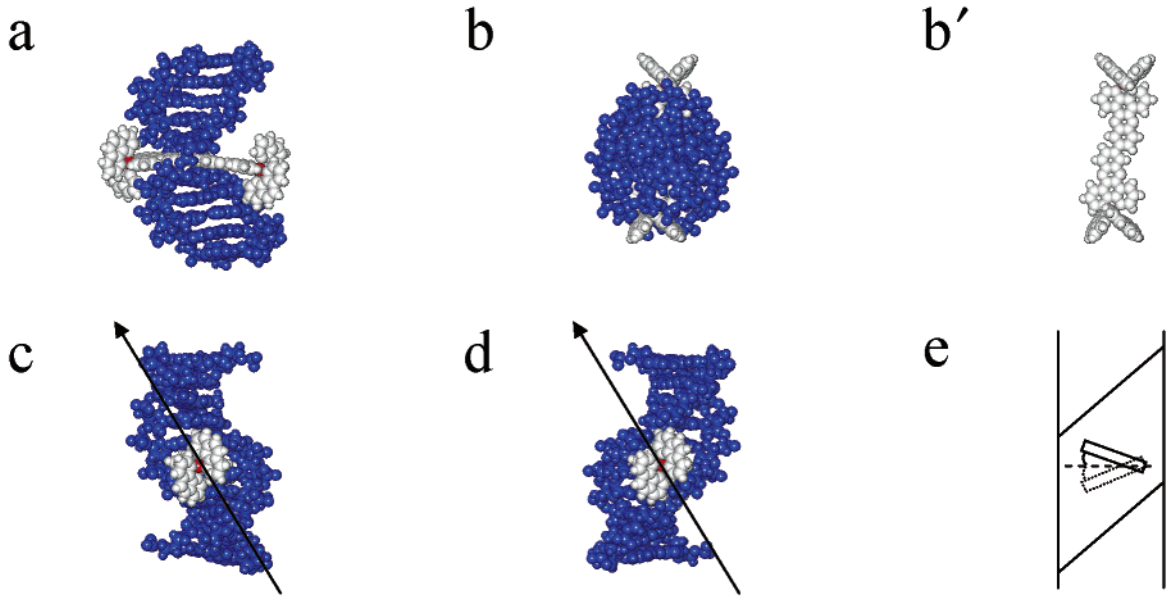

Figure 7. Model illustrating geometry of Δ,Δ-**1** at final binding in poly(dA-dT)$_2$. (a) View along 2-fold axis of Δ,Δ-**1** (minor groove to the left), (b) view along helix axis of the DNA showing asymmetric binding (to the right, complex viewed from top in absence of DNA), arrangement of the Ru(phen)$_2$ moieties in major (c) and minor groove (d) with B(A$_2$) phenanthroline transitions moments included. (e) Sense of roll defined as viewed into minor groove: intercalated dppz of minor groove bound Ru(phen)$_2$dppz moiety is rotated *clockwise* relative to perpendicularity to helix axis, while that of the Ru(phen)$_2$dppz moiety in the major groove is rotated *counterclockwise* as a consequence of twist around internuclear bond.

300 nm has to originate from the part that is not deeply intercalated. As mentioned above, this region of the spectrum is dominated by the B(A$_2$) phenanthroline transition (Figure 7c and d). A rotation of the part of the complex that is not deeply intercalated, around the pivotal 11−11′ bond (Figure 7e), would result in a more positive LD in the phenanthroline region for the meso form as the B(A$_2$) transition of the Δ moiety would get more parallel to the DNA helix axis, whereas the opposite would hold for the Λ moiety of the Λ,Λ form.

The even more positive LD in the phenanthroline region that can be observed for the Δ,Δ form when binding to poly(dA-dT)$_2$ (green curve, Figure 3b) may result from an even larger clockwise rotation of the part of the complex that is not deeply intercalated. We consider it more likely, though, that it is the orientation of the B(A$_2$) transition of the deeply intercalated part of Δ,Δ that is different from those of meso and Λ,Λ. As in the monomer parent compound, **3**, one could expect that the deeply intercalated part would be slightly tilted in a clockwise direction (Figure 7d).[26] This clockwise tilt would result in a more positive LD for a Δ moiety and a less positive LD for a Λ moiety. Thus, it is plausible that the three forms of **1** all have clockwise rotations of the two Ru(phen)$_2$ moieties that are situated in the grooves (Figure 7c,d).

It remains to be decided whether **1** binds with the bidppz ligand in a syn or anti conformation. The same LD effect as was observed in the phenanthroline region would be expected as a result of a small clockwise rotation of the Ru(phen)$_2$ moieties both for a syn and an anti conformation. One piece of evidence comes from the relatively strong, positive differential CD for the DNA-bound stereoisomers of **1** in the low-energy part of the visible region. The effect is much stronger than that for the monomer and seems associated with the threading binding mode for all three stereoisomers of **1**, as it is not seen in the initial, groove bound forms. It is therefore difficult to explain by anything else than an induced CD due to a chiral rotamer conformation of the bridging bidppz ligand. From calculations employing the PPP-CI-dipole velocity method,[47] we have found that the theoretical effect of an appropriately skewed (clockwise) syn conformation would be a negative CD in the low-energy part of the visible region, whereas an anti conformation rotated in a clockwise manner would result in a positive CD effect. Thus, we suggest that the bidppz ligand adopts an anti conformation when it is bound to DNA.

The great resemblance of the poly(dA-dT)$_2$ and poly(dI-dC)$_2$ results suggests that the final binding geometries of **1** in these polynucleotides are very similar. The generally lower quantum yields and luminescence lifetimes in ct-DNA and poly(dG-dC)$_2$ could be a result of the exocyclic amino group of guanine in the minor groove, not present in poly(dA-dT)$_2$ and poly(dI-dC)$_2$. The amino group prevents the complex from penetrating into the minor groove, and as a consequence, the aza nitrogens of the dppz moiety will be less protected from hydrogen bonding to water than when fully inserted between the nucleobases, resulting in more radiationless deactivation of the excited state. This supports that the luminescence properties mainly originate from the minor groove bound entity and thus that the metal center of the deeply intercalated part of the complex is indeed situated in the minor groove (as suggested in Figure 7). Another indication of a less deep (i.e., more symmetric) intercalation in poly(dG-dC)$_2$ is that the difference in LD in the phenanthroline region is small. A more symmetric intercalation could be expected to make the orientation of the Ru(phen)$_2$ moiety between the DNA bases less distinct and thus smear out the effect of clockwise rotation in LD. The difference between the stereoisomers in LD of **1** bound to ct-DNA in the phenanthroline region is also small. With ct-DNA, however, this could be a result of heterogeneity.

Further support for deep intercalation from the minor groove side comes from the comparison of the luminescence properties of the stereoisomers of **1** in poly(dA-dT)$_2$ and poly(dI-dC)$_2$ (Table 1). Δ,Δ-**1** displays similar luminescence lifetimes in poly-(dA-dT)$_2$ and poly(dI-dC)$_2$, suggesting that the structural change in the major groove, when going from poly(dA-dT)$_2$ to poly-(dI-dC)$_2$, is not important when a Δ moiety is situated in that groove. By contrast, the luminescence lifetimes of Λ,Λ-**1** in poly(dA-dT)$_2$ and poly(dI-dC)$_2$ differ significantly, suggesting that the structure of the major groove is important when a Λ moiety is situated in that groove. One possibility is then that

Λ,Λ-**1** is intercalated from the major groove and Δ,Δ-**1** from the minor groove. However, for meso-**1,** the LD spectra as well as luminescence lifetimes indicate that here the Λ moiety is preferably intercalated over Δ. Second, the luminescence lifetimes and the preexponential factors of meso-**1** are essentially the same in poly(dA-dT)$_2$ as in poly(dI-dC)$_2$, suggesting that, in contrast to Λ,Λ-**1**, the Λ moiety of the meso form is not in the major groove. In conclusion, meso-**1** intercalates its Λ moiety deeply in the minor groove and consequently has its Δ moiety in the major groove. The similarities in LD and luminescence lifetimes between meso- and Λ,Λ-**1**, finally suggest that one of the Λ moieties in Λ,Λ-**1** is indeed deeply intercalated from the minor groove side and that the differences in the luminescence lifetimes of Λ,Λ-**1** in poly(dA-dT)$_2$ and poly(dI-dC)$_2$ have to be explained by variations in interactions of the nonintercalated Λ-Ru(phen)$_2$dppz-moiety with the major groove. The molecular model in Figure 7 shows that also the nonintercalated half of the molecule may still be in close contact with the major groove, and thus, that a changed sense of chirality there can influence the intercalation geometry of the other, intercalated half.

Conclusions

The following has been learned about the binding modes of the ruthenium complex **1** in ct-DNA, poly(dA-dT)$_2$, poly(dG-dC)$_2$, and poly(dI-dC)$_2$:

1. The three stereoisomers of **1** are in all DNAs threaded through the DNA to reach their final intercalative binding geometries.

2. The initial, nonthreaded binding mode of Δ,Δ-**1** in ct-DNA, poly(dG-dC)$_2$, and poly(dI-dC)$_2$ is concluded to be in the major groove.

3. In poly(dA-dT)$_2$, no initial intermediate groove-bound species could be detected.

4. The initial binding sites of meso- and Λ,Λ-**1** in ct-DNA are in the major groove, although much more coplanar with the nucleobases than for the Δ,Δ enantiomer.

5. The final binding geometry of the three stereoisomers of **1** in poly(dA-dT)$_2$ is characterized by the bidppz ligand being intercalated between the nucleobases in an anti conformation, with a small rotation around the central pivot bond. The complex intercalates asymmetrically, with one of the Ru(phen)$_2$ moieties deeply situated in the minor groove.

6. The meso stereoisomer provides a probe of stereoselectivity. The Λ part is concluded to be deeply intercalated from the minor groove, probably a result of a better fit of the Δ part in the major groove.

Acknowledgment. Dr. Gunnar Stenhagen is acknowledged for the ES-MS measurements. This project was funded by The Swedish Research Council (VR).

Supporting Information Available: Figures displaying the differential CD spectra of compounds used. This material is available free of charge via the Internet at http://pubs.acs.org.

References and Notes

(1) Watson, J. D.; Crick, F. H. C. *Nature* **1953**, *171*, 737.
(2) Müller, W.; Crothers, D. M. *J. Mol. Biol.* **1968**, *35*, 251.
(3) Liaw, Y. C.; Gao, Y. G.; Robinson, H.; Vandermarel, G. A.; Vanboom, J. H.; Wang, A. H. J. *Biochemistry* **1989**, *28*, 9913.
(4) Gao, Y. G.; Liaw, Y. C.; Robinson, H.; Wang, A. H. J. *Biochemistry* **1990**, *29*, 10307.
(5) Egli, M.; Williams, L. D.; Frederick, C. A.; Rich, A. *Biochemistry* **1991**, *30*, 1364.
(6) Smith, C. K.; Davies, G. J.; Dodson, E. J.; Moore, M. H. *Biochemistry* **1995**, *34*, 415.
(7) Collier, D. A.; Neidle, S.; Brown, J. R. *Biochem. Pharmacol.* **1984**, *33*, 2877.
(8) Williams, L. D.; Egli, M.; Qi, G.; Bash, P.; Vandermarel, G. A.; Vanboom, J. H.; Rich, A.; Frederick, C. A. *Proc. Natl. Acad. Sci. U.S.A.* **1990**, *87*, 2225.
(9) Fox, K. R.; Waring, M. J. *Biochim. Biophys. Acta* **1984**, *802*, 162.
(10) Fox, K. R.; Brassett, C.; Waring, M. J. *Biochim. Biophys. Acta* **1985**, *840*, 383.
(11) Sun, D. Y.; Hansen, M.; Clement, J. J.; Hurley, L. H. *Biochemistry* **1993**, *32*, 8068.
(12) Sun, D. Y.; Hansen, M.; Hurley, L. *J. Am. Chem. Soc.* **1995**, *117*, 2430.
(13) Hansen, M.; Hurley, L. *J. Am. Chem. Soc.* **1995**, *117*, 2421.
(14) Bourdouxhe-Housiaux, C.; Colson, P.; Houssier, C.; Waring, M. J.; Bailly, C. *Biochemistry* **1996**, *35*, 4251.
(15) Önfelt, B.; Lincoln, P.; Nordén, B. *J. Am. Chem. Soc.* **1999**, *121*, 10846.
(16) Önfelt, B.; Lincoln, P.; Nordén, B. *J. Am. Chem. Soc.* **2001**, *123*, 3630.
(17) Friedman, A. E.; Chambron, J.-C.; Sauvage, J.-P.; Turro, N. J.; Barton, J. K. *J. Am. Chem. Soc.* **1990**, *112*, 4960.
(18) Balzani, V.; Ballardini, R. *Photochem. Photobiol.* **1990**, *52*, 409.
(19) Pyle, A. M.; Barton, J. K. *Prog. Inorg. Chem.* **1990**, *38*, 413.
(20) Friedman, A. E.; Kumar, C. V.; Turro, N. J.; Barton, J. K. *Nucleic Acids Res.* **1991**, *19*, 2595.
(21) Jenkins, Y.; Friedman, A. E.; Turro, N. J.; Barton, J. K. *Biochemistry* **1992**, *31*, 10809.
(22) Chow, C. S.; Barton, J. K. *Methods Enzymol.* **1992**, *212*, 219.
(23) Hiort, C.; Lincoln, P.; Nordén, B. *J. Am. Chem. Soc.* **1993**, *115*, 3448.
(24) Haq, I.; Lincoln, P.; Suh, D. C.; Nordén, B.; Chowdhry, B. Z.; Chaires, J. B. *J. Am. Chem. Soc.* **1995**, *117*, 4788.
(25) Nordén, B.; Lincoln, P.; Åkerman, B.; Tuite, E. In *Metal Ions In Biological Systems*; Siegel, A., Siegel, H., Eds.; Marcel Dekker: New York, Basel, Hong Kong, 1996; Vol. 33, p 177.
(26) Lincoln, P.; Broo, A.; Nordén, B. *J. Am. Chem. Soc.* **1996**, *118*, 2644.
(27) Erikkila, K. E.; Odom, D. T.; Barton, J. K. *Chem. Rev.* **1999**, *99*, 2777.
(28) Tuite, E.; Lincoln, P.; Nordén, B. *J. Am. Chem. Soc.* **1997**, *119*, 239.
(29) Dupureur, C. M.; Barton, J. K. *J. Am. Chem. Soc.* **1994**, *116*, 10286.
(30) Önfelt, B.; Lincoln, P.; Nordén, B.; Baskin, J. S.; Zewail, A. H. *Proc. Natl. Acad. Sci. U.S.A.* **2000**, *97*, 5708.
(31) Önfelt, B.; Olofsson, J.; Lincoln, P.; Nordén, B. *J. Phys. Chem. A* **2003**, *107*, 1000.
(32) Jacquet, L.; Kirsch-De Mesmaeker, A. *J. Chem. Soc.-Faraday Trans.* **1992**, *88*, 2471.
(33) Moucheron, C.; Kirsch-De Mesmaeker, A.; Choua, S. *Inorg. Chem.* **1997**, *36*, 584.
(34) Staffilani, M.; Belser, P.; De Cola, L.; Hartl, F. *Eur. J. Inorg. Chem.* **2002**, 335.
(35) Staffilani, M.; Belser, P.; Hartl, F.; Kleverlaan, C. J.; De Cola, L. *J. Phys. Chem. A* **2002**, *106*, 9242.
(36) Bilakhiya, A. K.; Tyagi, B.; Paul, P.; Natarajan, P. *Inorg. Chem.* **2002**, *41*, 3830.
(37) Lincoln, P.; Nordén, B. *Chem. Commun.* **1996**, 2145.
(38) Wilhelmsson, L. M.; Westerlund, F.; Lincoln, P.; Nordén, B. *J. Am. Chem. Soc.* **2002**, *124*, 12092.
(39) Reference 36 gives an ϵ being a factor 2 too low.
(40) Nordén, B.; Kubista, M.; Kurucsev, T. *Q. Rev. Biophys.* **1992**, *25*, 51.
(41) Lakowicz, J. R. *Principles of Fluorescence Spectroscopy*; Plenum Press: New York, 1983; p 112.
(42) Ardhammar, M.; Lincoln, P.; Rodger, A.; Nordén, B. *Chem. Phys. Lett.* **2002**, *354*, 44.
(43) CD_{diff} reflects changes of the intrinsic CD of the chiral chromophore upon interaction with the (chiral) DNA environment, including what is generally denoted as "induced CD".[44]
(44) Eriksson, M.; Nordén, B. *Methods Enzymol.* **2001**, *340*, 68.
(45) "Quasi-intercalation" is a hypothetical binding model (proposed in ref 46) in which the DNA double helix does not unwind. A polycyclic aromatic moiety may according to this binding model be stabilized by sharing overlap with the coplanar base pairs above and below the binding site.
(46) Lincoln, P.; Nordén, B. *J. Phys. Chem.* **1998**, *102*, 9583.
(47) Harada, N.; Nakanishi, K. *Circular Dichroism Spectroscopy − Exciton Coupling in Organic Stereochemistry*; University Science Books − Oxford University Press: Oxford, 1983.